THE EUROPEAN
PHYSICAL JOURNAL C

Light dark matter axion-wind detection with a static electric field

Yu Gao[1,a] , Yongsheng Huang[2], Zhengwei Li[1], Manqi Ruan[1,3], Peng Sha[1], Meiyu Si[1,3] , Qiaoli Yang[4,b]

[1] Institute of High Energy Physics, Chinese Academy of Sciences, Beijing 100049, China
[2] School of Science, Shenzhen Campus of Sun Yat-sen University, Shenzhen 518107, China
[3] University of Chinese Academy of Sciences, Beijing 100049, China
[4] Physics Department and Siyuan Laboratory, Jinan University, Guangzhou 510632, China

Abstract We explore the axionic dark matter search sensitivity with a narrow-band detection scheme aimed at the axion-photon conversion by a static electric field inside a cylindrical capacitor. An alternating magnetic field signal is induced by effective currents as the axion dark matter wind flows perpendicularly through the electric field. At low axion masses, such as in a KKLT scenario, front-end narrow band filtering is provided by using LC resonance with a high Q factor, which enhances the detectability of the tiny magnetic field signal and leads to thermal noise as the major background that can be reduced under cryogenic conditions. We demonstrate that high $g_{a\gamma}$ sensitivity can be achieved by using a strong electric field $E \sim$ MVm^{-1}. The QCD axion theoretical parameter space would require a high $E \sim$ GVm^{-1} field strength. Using the static electric field scheme essentially avoids exposing the sensitive superconducting pickup to an applied laboratory magnetic field.

1 Introduction

Astrophysical and cosmological observations indicate the existence of cold dark matter as 23% [1] of the Universe's total energy budget. Promising scenarios include dark matter in the form of extralow mass bosons [2], and one highly motivated candidate is the axion [3–10]. Naturally relaxing the amount of Charge-Parity violation in the Standard Model's strong interaction [11,12] (a.k.a. the strong CP problem [13]), the axion emerges from a natural global $U(1)_{PQ}$ symmetry extension of the Standard Model (SM), which is spontaneously broken at high scale and later explicitly broken at the strong interaction's confinement scale by the QCD instanton potential [14,15], making the axion a pseudo-Nambu-

Goldstone particle with a small but non-zero mass. Cosmologically, through the 'misalignment' mechanism [16–21] axions are produced during the QCD phase transition and their collective evolution makes up the dark matter density observed at the current time. Depending on the spontaneous $U(1)_{PQ}$ breaking scale relative to that of inflation, typically cosmic axions account for the relic density in the classical mass window with $m_a \sim \mathcal{O}(10^{-5} - 10^{-3})$ eV [21] or $m_a < \mathcal{O}(10^{-7})$ eV [22], and a wider dark matter axion mass range is possible through other production mechanisms.

The axion acquires its characteristic $\frac{a}{f_a}G\tilde{G}$ coupling through a loop of $SU(3)_c$-charged fermions, such as in benchmark invisible axion scenarios such as the KSVZ [7,8] and the DFSZ [9,10] models. Generally the axion can also couple to other SM gauge fields, in particular the QED photon, with the interaction Lagrangian term

$$\mathcal{L}_{a\gamma\gamma} = g_{a\gamma}a\vec{E} \cdot \vec{B}, \tag{1}$$

where $\vec{E}, \vec{B}$ are the electric and magnetic field strengths, the axion-photon coupling is $g_{a\gamma} = c_\gamma \alpha_{QED}/(\pi f_a)$, with f_a as the $U(1)_{PQ}$ symmetry's scale factor, $\alpha_{QED} = 1/137$ is the fine-structure constant and the $\mathcal{O}(1)$ coefficient c_γ is given by the details of the particular UV model. This coupling also characterizes the generalized axion-like particles (ALPs), which can be created from dimension compactification in string theory, or other UV theories with an extra light bosonic mode that may not necessarily couple to the SM gluon field. General ALPs have relaxed $f_a - m_a$ correlation compared to that of the QCD axion, thus they have a much wider parameter space to serve as a dark matter candidate. In the following we use 'axion' to denote both the QCD axion and ALPs if not specified.

The axion-photon coupling $g_{a\gamma}$ allows the dark matter axion to convert into photons inside a laboratory's electromagnetic fields, and is being actively searched for by

[a] e-mail: gaoyu@ihep.ac.cn (corresponding author)

[b] e-mail: qiaoliyang@jnu.edu.cn (corresponding author)

cavity haloscopes including ADMX [23], HAYSTAC [24], CAPP [25], ORGAN [26], CAST-RADES [27], QUAX-$a\gamma$ [28], TASEH [29], DANCE [30], noncavity experiments such as ABRACADABRA [31], high-frequency dielectric design such as MADMAX [32], BREAD [33], and many others. For recent reviews of axion search methods, see Refs. [34,35]. To date, resonant cavity haloscopes have achieved the highest sensitivity due to the high-Q front-end enhancement at both classical [36] and quantum levels [37]. However, matching the signal photon's wavelength in the low axion mass range $m_a \ll 10^{-6}$ eV, motivated by string theory [38], GUT scale new physics [39–43], etc., faces the practical limitation of cryogenic equipment sizes. For a low axion mass the size of the resonant cavity could be too large, and multiple promising complementary methods are helpful, such as in ABRACADABRA [31], SHAFT [44], ADMX-SLIC [45], BASE [46], and DMRadio [47], each featuring different strengths and limitations.

From the theoretical perspective, the $m_a \lesssim 10^{-7}$ eV axion does have unique attractions. It has been shown that very light axions have strong implications for inflation [22]. Models with a very light axion typically have a PQ symmetry breaking scale f_a order of the GUT scale, which results in considerable tensions between the observed isocurvature fluctuations and high-scale inflation. A low energy scale inflation scenario will be necessary if very light dark matter axions are detected. The discovery of very light dark matter axions will also indicate the observed Universe as a highly atypical Hubble volume and possibly the KKLT scenario [22]. Thus, for low-mass axions, an alternative detection method has been proposed in Refs. [48,49] to utilize the high Q-factor of a resonant LC circuit as a narrow-band pickup. Following this idea, dark matter experiments with LC-enhanced pickup systems have been carried out [31,47,49]. However the very strong magnetic fields created by magnets or solenoids inherently possess small fluctuations which would be hard to separate from the tiny axion induced signals.

In this paper, we propose a narrow-band axion dark matter experimental scheme based on an electrified cylindrical capacitor. We investigate the prospective sensitivity to axion-photon coupling $g_{a\gamma}$ with a resonance circuit as the high Q pickup of induced signals from axion coupling to a strong laboratory electric field. In comparison with using a strong magnetic field as the conversion medium, while the axion-to-photon conversion rate inside an electric field is suppressed by the subunity local dark matter velocity, using the $\vec{E}$ field [50] can avoids placing a sensitive magnetic probe close to a strong magnetic field. In addition, the signal strength with an electric field is modulated by the relative angle of the $\vec{E}$ field orientation and the direction of the local dark matter flux, which provides a potential test of the origin of a signal.

In Sect. 2, we describe the experimental schematics with a meter-scale cylindrical capacitor, and calculate the signal

strength of the DM axion-induced signal with an LCR resonance pickup. Section 3 discusses the major noises and the prospective sensitivity in an axion mass range $m_a < 10^{-6}$ eV. We demonstrate that good axion-photon coupling sensitivity can be achieved with a static electric field as the converting medium, and then we conclude in Sect. 4.

2 Cylindrical capacitor setup

For terrestrial laboratories, the dark matter axion can be modeled as a plane wave

$$a(x, t) \approx a_0 \cos\left[m_a \vec{v}_a \cdot \vec{x} - \left(m_a + \frac{m_a}{2}v_a^2\right)t\right], \qquad (2)$$

with a de-Broglie wavelength $\lambda_a = k_a^{-1} \sim (v_a m_a)^{-1}$. $v_a \sim 10^{-4} - 10^{-3}$ is the Earth's relative velocity to the local bulk of the galaxy's dark matter halo, and the local dark matter forms an 'axion wind' to the Earth. The local axion field magnitude is $a_0 = \sqrt{2\rho_{\mathrm{DM}}}/m_a$ where the local DM halo density is typically $\rho_{\mathrm{DM}} = 0.4$ GeV cm^{-3}. For λ_a longer than the dimension of the experimental apparatus, this axion field can be considered a coherent classical background field [51,52] that oscillates at $\omega_a = (1 + v_a^2/2)m_a$, for which the axion velocity can interchange with the axion field's spatial gradient up to a small red(blue)-shift due to Earth's motion. The energy spread due to the halo velocity dispersion is usually small, and it is often denoted by the axion field quality factor as $\delta\omega_a/\omega_a \equiv Q_a^{-1}$. For conventional dark matter halo models [20], $Q_a \sim 10^6$, any signals from this nearly monochromatic oscillation would be efficiently detected from a narrow-band probe with a matched quality factor.

When the axion is considered as a background field, the axion-modified Maxwell equations [36] observe the addition of an effective 4-current density $j^\mu = \{\vec{\nabla}a \cdot \vec{B}, -g_{a\gamma}\vec{E} \times \vec{\nabla}a + g_{a\gamma}\dot{a}\vec{B}\}$ that simplifies to an effective displacement current density $\vec{j}_a$ inside a static laboratory electric field. The modified Maxwell equations are

$$
\begin{aligned}
\vec{\nabla} \cdot \vec{E} &= \rho_e, \\
\vec{\nabla} \times \vec{B} - \frac{\partial \vec{E}}{\partial t} &= \vec{j}_e + \vec{j}_a, \\
\vec{\nabla} \cdot \vec{B} &= 0, \\
\vec{\nabla} \times \vec{E} &= -\frac{\partial \vec{B}}{\partial t},
\end{aligned}
\qquad (3)
$$

where $\vec{E} = \vec{E}_0 + \vec{E}_a$ is dominated by the static field $\vec{E}_0$ and $\vec{j}_e = 0$. $\vec{j}_a = -g_{a\gamma}a\vec{E}_0 \times \vec{k}_a$ alternates at the same frequency as the axion field, and it induces a magnetic field signal $\vec{B}_a$. Since $\vec{j}_a$ is perpendicular to both $\vec{E}$ and $\vec{v}_a$, $\vec{j}_a$ depends on the angle between the local dark matter density flow density and the applied field $\vec{E}_0$. This will lead to periodic $\vec{j}_a$

modulations, for instance, at a 24-hour period due to the Earth's rotation that orientate the apparatus to the direction of the local dark matter flow. Another shorter-period modulation over $2\pi(v_a\omega_a)^{-1}$ also arises as the nonrelativistic axion field may have a longer wavelength $\lambda_a = (\beta m_a)^{-1}$ than the size of the $\vec{E}_0$-field region, which causes the strength of $\vec{\nabla}a$ to fluctuate as the a field propagates. We also note that the amplitude $j_a = g_{a\gamma}\sqrt{2\rho_{\mathrm{DM}}} \cdot |\vec{v}_a \times \vec{E}_0|$ is insensitive to m_a for a given dark matter energy density.
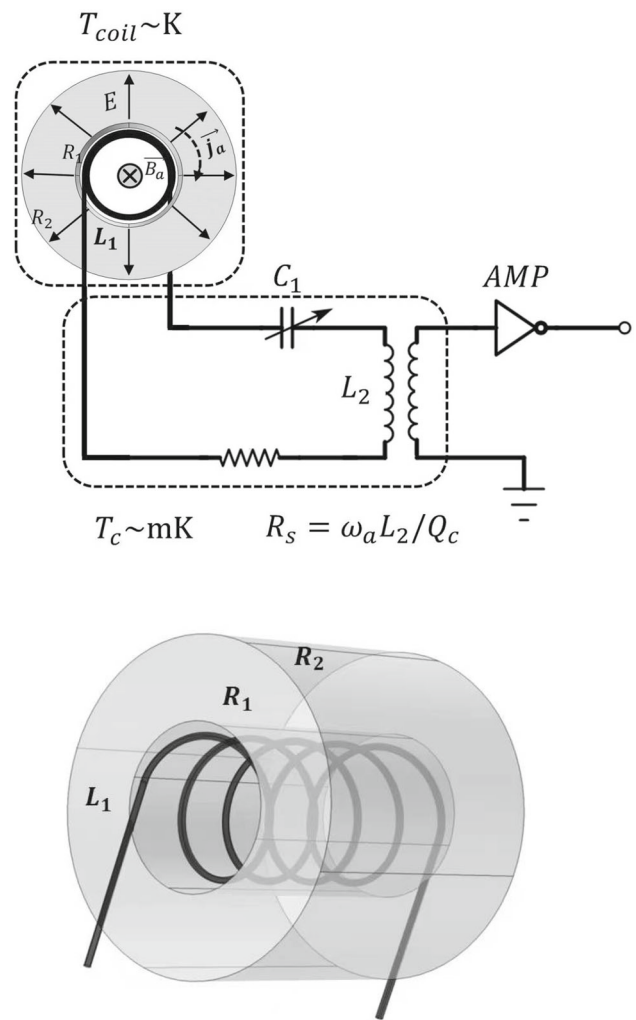
With a cylindrical capacitor, as illustrated in Fig. 1, and assuming $\vec{a}$ is along the cylinder axis, $\vec{j}_a$ is circularly distributed in the radial $\vec{E}$-field region between the capacitor plates, forming an effective current loop and the induced magnetic field amplitude along the cylinder axis [50] is

$$B_a = g_{a\gamma}E_0 v_{\mathrm{DM}} c_R \sqrt{2\rho_{\mathrm{DM}}} R_1$$
$$\sim 2 \times 10^{-10}\mathrm{T} \cdot \left(\frac{g_{a\gamma}}{\mathrm{GeV}}^{-1}\right)\left(\frac{E_0}{10^7\mathrm{V/m}}\right)\left(\frac{R_1}{0.1\mathrm{m}}\right),$$
(4)

where R_1 is the inner radius of the capacitor and E_0 denotes the strongest electric field strength at the inner radius. c_R is an $\mathcal{O}(1)$ parameter determined by the geometry of the capacitor cross-section. $v_{\mathrm{DM}} = 10^{-4}$ is the Earth's local relative velocity to the dark matter halo.

In a simplified low-frequency and long-solenoid limit, the signal magnetic field can be easily computed by integrating out the total effective current between the capacitor's inner and outer radii, and the form factor is $c_R = \ln(R_2/R_1) = 0.69$ for $R_2 = 2R_1$. The realistic evaluation of $c_R(\omega)$ can be much more involved, which depends on the axion oscillation frequency, radius-length ratio, plate thickness and material, etc. Here we resort to numerical electromagnetic simulation with the Comsol package. For a sample study, we choose the geometry with $R_2 = 2R_1$ and a cylinder length equal to twice of R_2. We performed simulations with 5 mm-thick nonconductor material plates and assuming the capacitor was placed inside a shielding box. Simulations show that c_R at low frequencies is a constant value around 0.3, mostly due to the large opening at the cylinder's ends, which spoils the long-solenoid symmetry [53] and lets the induced magnetic field be on both the inside and outside of the cylinder; the expected frequency-dependence from decoherence starts to show up near the cut-off frequency, as shown in Table 1. We will assume a similar c_R behavior with the frequency fraction f/f_{max} to give sensitivity estimate at our benchmark cases, which scale up with the same ratio of dimensions. In principle c_R could be improved with a longer cylinder; we will postpone the geometric optimization of c_R for future work.

An N_1-turn coil of radius $R_{\mathrm{coil}} \sim R_1$ is then placed in the central region of the capacitor to pick up the induced magnetic flux $\Phi_a = B_a \cdot \pi R_1^2$. This magnetic flux corresponds

Fig. 1 Illustrative experiment setup. Upper: a superconductor coil L_1 is placed in the central region of a cylindrical capacitor, and is connected in a resonant LCR circuit as a narrow-band pickup for the axion-induced signal $\vec{B}_a$. The inner layer (R_1) of the capacitor should be non-conducting to let in the induced signal. R_s denotes the total resistance. Lower: The pickup coil L_1 is loosely winded to reduce its self-inductance and allows the signal to penetrate into the central region. Using superconducting L_1 and L_2 can lower their resistance and reduce thermal noise

Table 1 Simulated c_R values at different frequencies, $R_2 = 2R_1 = 0.4$ m and $f_{\mathrm{max}} = 0.1875$ GHz. The cylinder length is set to 0.8 m, corresponding to Benchmark A in Sect. 3. The cylinder assumes 5 mm nonconductive material plates and they are enclosed inside an exterior shielding box

f/f_{max}	$< 10^{-3}$	0.07	0.34	0.67	6.7
c_R	0.283	0.257	0.218	0.150	0.120

to the B_a component parallel to the cylinder axis, and is proportional to the $v_{a,z}$ component along $\hat{z}$; the $\vec{v}_a$ projections in the $\hat{x}$ and $\hat{y}$ directions do not contribute to Φ_a. In our calculations, we assume $\vec{v}_a // \hat{z}$, while in measurement $\vec{v}_a \cdot \hat{z}$ yields

a directional dependence in Φ_a that in principle can be used as check by adjusting the experiment's orientation.

The pickup coil is connected as part of an LCR circuit with its resonance point tuned to a target search frequency of the axion field oscillation, e.g. $LC = \omega^{-2}$. The total inductance L (without subscript) includes contributions from the pickup coil L_1, the effective inductance L_2 of the inductive coupling to amplifier circuit and any additional inductance from wiring. L_2 includes both the coupled coils' self-inductance and mutual inductance. We would require $L_1 \gg L_2$ to ensure $L \sim L_1$. Note that a single-turn circular loop with wire radius $d_1 \sim$ mm has a self-inductance approximately 10μH per meter. The pickup coil L_1 can be loosely winded to reduce the inductance between its adjacent turns, so that $L_1 \propto N_1$. The LCR resonance requires a capacitance value $C = (2\pi f)^{-2}/L \sim 0.3$pF $\cdot (\mu$H$/L) (0.1$ GHz$/f)^2$, which increases toward lower axion mass, and is much larger than typical stray capacitance on meter-scale wiring. Low-temperature tuning of the LCR resonance frequency can be achieved via an adjustable capacitor.

As the signal strength derives from one pickup loop's enclosed magnetic flux, which are 2D quantities, Eq. (4) seems to have no explicit dependence on the cylinder's length. However, the cylinder length still affects how many turns N_1 can loosely wind into the pickup, and it is also coherence limited by the signal photon's half-wavelength [54], and appears in the theoretical upper limit of the axion-photon coherent conversion rate.

The high LCR quality factor at its resonance point allows for an enhanced current in the circuit [49]. The saturated current in the loop is

$$I_a = Q_c \cdot (\pi R_1^2 N_1 B_a L^{-1}) \cos \omega t, \qquad (5)$$

where Q_c denotes the conventional LCR quality factor $Q_c = \omega_a L / R_s$. The signal power is stored in the LCR circuit utill the energy dissipation power by the resistance is $P_{\text{dis.}} = Q_c \cdot (N_1 \Phi_a / L)^2 \omega_a L / 2$ equals that of the signal feed. For efficient signal pickup, Q_c should match the order of magnitude of the quality factor in the axion field $Q_c \sim Q_a$, which also matches the saturated energy dissipation to the dark matter axion-photon energy conversion rate. Here we choose $Q_c \sim Q_a$ for a proof-of-principle estimate. In practice, Q_c should be replaced by a 'loaded' quality factor after coupling to the amplifier/detector chain, and further optimization is needed [55,56]. Note that for a high Q_c, saturating the maximal current takes Q_c oscillation periods, and in the MHz–GHz range it is typically much shorter than the time scale of $\vec{v}_a$ variation. However, in principle it could require significantly longer time $Q_c \cdot 2\pi \omega_a^{-1}$ in the case of extremely low axion masses. In the MHz~GHz range, the saturation time is less than a second and we consider that the maximal LCR current is always reached during the observation time.

The inner volume of the cylindrical capacitor, along with the pickup circuit, is placed under cryogenic conditions to suppress thermal noise. Environmental fluctuations can be removed via electromagnetic shielding. Since there is no strong magnetic field in the system, the inductance coils and the capacitor in the LCR loop can be made with superconductor materials, such that the circuit components with the major resistance can be confined to a small spatial region and placed under an extreme cryogenic temperature, $T_c \sim$ mK. This reduces the cooling requirement on the sizable superconducting pickup L_1, without worsening its noise. For instance, the NbTi superconductor has a transition temperature at 9.7 K and has a good transmission rate for 10^2 MHz signals. Denoting R_s as the total resistance in the LCR circuit, a low effective resistance on the superconducting NbTi pickup coil $R_{\text{coil}} \ll R_s$ would allow a much higher temperature $T_{\text{coil}} = T_c \cdot (R_s/R_{\text{coil}})$ and keep the coil's thermal noise subdominant. Note for a meter-radius, loosely winded 10 round loop, $L_1 \sim 50 - 100\mu$F and the LCR resonance requires $R_s = \omega L/Q_c = 0.04\Omega \cdot (f/GHz)$. The contact resistance can be reduced to 10^{-3} Ω. If L_1 is at 1 K with the rest of the LCR at mK, L_1's effective resistance needs to be controlled to $R_{\text{coil}} < 10^{-5}$ Ω.

3 Noise and sensitivity

The induced current $I_a(t)$ in the LCR circuit is then coupled to the amplifier/detector chain. The leading current noise in the LCR is Johnson-Nyquist noise due to the resistance in the LCR circuit, $\delta I^2 = k_B T_c \Delta f / R_s$. This noise will also be amplified at the subsequent amplifier(s) and can be the major noise in signal measurement. The total noise power is

$$P_n = k_B T_c \Delta f + k_B T_D \Delta f, \qquad (6)$$

where the latter is an equivalent readout noise power that includes the added noises from amplifier and detector chain, etc. For the detection bandwidth we take $\Delta f = Q_c^{-1} f$ as a reasonable estimate. High sensitivity and low dissipation amplification help maintain the SNR from the LCR loop. For instance, using a SQUID to convert the inductively coupled $I_a(t)$ into a voltage signal is proposed in Ref. [49], and other amplifications are possible. State-of-the-art cryogenic detectors such as the HEMT have $T_D \sim K$ noise temperature. Recent developments in interferometry techniques can further reduce the detector noise level to $T_D \leq 0.1$ K [57,58] and are applicable in axion search [37,59]. With sufficient amplification it is possible for the amplified JN noise to be larger than the added detector noise. Thus for a proof-of-principle analysis in this paper, we take $T_c = 1$ mK and 10 mK as benchmark scenarios and assume that the pickup circuit's thermal noise dominates after amplification.

Assuming thermal noise dominates after amplification, the SNR for the signal with I_a^2 and δI^2 is

$$
\begin{aligned}
\mathrm{SNR} &= \frac{(Q_c N_1 \Phi_a / L)^2 R_s}{2 k_B T_c} \sqrt{\frac{t}{\Delta f}} ,\\
&= \frac{Q_c (N_1 \cdot \pi R_1^2 B_a)^2}{2 L k_B T_c} \sqrt{Q_c \cdot 2\pi \omega_a \cdot t}
\end{aligned}
\tag{7}
$$

where t is the integrated total observation time, g is the effective signal power gain from subsequent amplifiers, and we used the relation $R_s = L\omega_a / Q_c$ at the resonance frequency. This SNR formula is similar to that of a resonant cavity haloscope in the sense of a high Q enhancement from front-end frequency filtering on the near-monochromatic signal. Note that in Eq. (7) the integrated time t is typically longer the than axion field's coherent time-scale $t_c = 2\pi Q_c / \omega_a \approx (m_a v_a^2)^{-1}$, and the latter is from 10^{-2} s up to a few minutes for m_a between 10^{-10} eV and 10^{-6} eV. In experiments such as ADMX [60] and ADMX-SLIC [45], data-taking is on a time-scale comparable to t_c and then repeated. The repeated $N_{\mathrm{obs.}} = t/t_c$ times of measurement reduce the statistical uncertainty in the noise power by $1/\sqrt{N_{\mathrm{obs.}}}$. Since the signal power $\propto g_{a\gamma}^2$, the sensitivity of the axion-photon coupling then scales as $g_{a\gamma} \propto (t/t_c)^{-1/4}$. Recently, dedicated detector-specific analyses [61,62] have been performed for continuous measurement over $t > t_c$, showing a consistent $g_{a\gamma} \propto (t/t_c)^{-1/4}$ relation for long data-taking times [63]. Without going into detector/amplifier details, in this paper, we will consider the average signal power measurement as a sensitivity estimate.

The shaded benchmark regions in Fig. 2 demonstrate the narrow-band sensitivity in the applicable frequency range of the experimental setup. Incremental narrow-band measurements need to be performed at frequency intervals of $\Delta f = m_a / Q$ and it typically takes time to scan a significant frequency range. For $t > t_c$, the sensitivity scales as $g_{a\gamma} \propto t^{-1/4}$, so that a shorter integration time at each frequency can also yield meaningful results. For instance, reducing t to 1 h will reduce the plotted sensitivities by a factor of 3.6.

In Eq. (7), lowering L helps but it is related to the pickup loop's own geometry. When the L_1 coil is loosely winded, $L \approx N_1 \times R_1 [\ln(8R_1/r_1) - 2]$ and the SNR still benefits from increasing the turn number N_1 if L_1 dominates the total L. We take modest numbers $N_1 = 5, 10$ as it is desirable to have a large R_1 to maximize the pickup area. The benchmark selections of experimental parameters are given in Table 2. Demanding SNR=3 and observation time t on one frequency point, the sensitivity on the axion-photon coupling is

$$
g_{a\gamma} = \frac{\sqrt{\mathrm{SNR} \cdot 2 N_1 L_{1,0} \cdot k_B T_c}}{(\pi R_1^3 N_1 E_0 v_a c_R \sqrt{2\rho_{\mathrm{DM}}}) \sqrt[4]{Q_c^3 \, 2\pi \omega_a t}} ,
$$
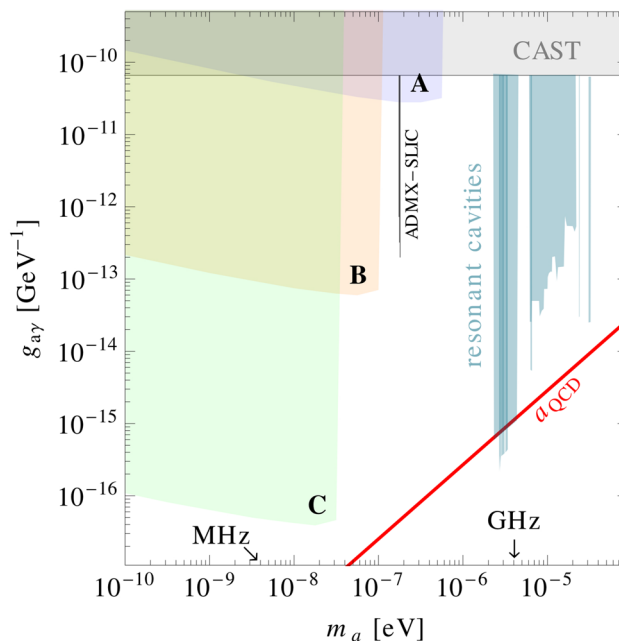
Fig. 2 Prospective single-frequency sensitivity with benchmark parameter sets listed in Table 2. The projected $g_{a\gamma}$ sensitivities (dotted lines) assume one week of observation time at each frequency, and the maximal m_a corresponds to the axion field coherence limit that $\lambda_\gamma > 8R_1$. The shaded regions (A, B, C) represent the applicable parameter space, rather than the frequency coverage in one single narrow-band measurement. The CAST limit (gray, top) and recent results from cavity haloscopes (vertical, right) and ADMX-SLIC (vertical, middle) are shown for comparison. The red solid line denote the theoretical predicted axion-photon coupling strength in the KSVZ model

$$
\approx 1.4 \times 10^{-12} \ \mathrm{GeV}^{-1} \left(\frac{R_1}{1 \ \mathrm{m}}\right)^{-3} \left(\frac{E_0}{\mathrm{MV}} m^{-1}\right)
$$
$$
\times \left(\frac{m_a}{10^{-6} \ \mathrm{eV}} \cdot \frac{t}{\mathrm{hr}}\right)^{-1/4} \left(\frac{N_1}{5}\right)^{-1/2} \left(\frac{T_c}{10 \ \mathrm{mK}}\right)^{1/2} ,
\tag{8}
$$

where we take $v_a = 10^{-4} c$, $N_1 = 5$, c_R interpolated from Table 1 and $L_{1,0} \equiv L_1/N_1 \sim \mu H$ which represents the inductance per turn. The sensitivity reach with benchmark parameters is illustrated in Fig. 2, where the sensitivity curves assume one week of integration time at each scanned frequency. As a narrow-band measurement, short-step frequency scanning is necessary, and resonance frequency tuning can be achieved by adjusting the capacitor's capacitance in the LCR circuit. In practice, the measurement bandwidth at each frequency may need to balance between the dark matter's intrinsic $m_a \cdot Q_a^{-1}$ and the practical bandwidth of the readout system. A reasonable strategy would be choosing a frequency below the cut-off frequency, where the projected sensitivity is relatively high, then scan a neighborhood around this frequency.

Benchmark A assumes modest parameter values that can fit into conventional dilution fridges, and for $t \sim 1$ week

Table 2 Benchmark setups. Common parameters include $Q_c \sim 10^6$, $\rho_{DM} = 0.4$ GeV cm^{-3}, and pickup wire radius $r_1 = 1$ cm. The corresponding $g_{a\gamma}$ sensitivity is shown in Fig. 2

Benchmark	R_1 (m)	N_1	E (V/m)	T_c (mK)
A	0.2	5	3×10^6	10
B	1	10	10^7	1
C	3	20	10^9	1

observation time, the sensitivity dips below the current solar axion search constraint [64] at the optimal frequency of approximately 0.2 GHz. Note that the sensitivity reach is for a single-frequency measurement, and scanning over a finite neighborhood of m_a requires spending an total observation time t at each frequency point, with intervals at $Q_c^{-1} m_a$. Benchmark B assumes more aggressive cryogenic conditions for a multimeter cylinder and the projected sensitivity can reach $g_{a\gamma} \sim 3 \times 10^{-15}$ GeV^{-1} at $m_a = 0.1$ μeV, or 19 MHz. Here we use an MVm^{-1} field strength above air's breakdown limit as a reasonably strong E field. $E > 30$ Vm^{-1} is achieved in modern high-voltage cavities [65,66], and voltage tolerance can be improved with insulator coating on capacitor plates and applying high vacuum [67,68]. Implementation under cryogenic conditions requires high-voltage R&D at the engineering level. Electric leakage in principle contributes a short noise and its shielding needs further investigation. One also needs to consider the breakdown limit of the electric-field strength in the capacitor. For semiconductors, Ref. [69] found that the breakdown field strength of ultrathin atomic-layers is approximately 30 MV/cm, and the leakage current density between GaAs and Au is low, approximately 10^{-10}A/cm^2, which should not be a concern if we consider a modest vacuum level. For instance, the electrical breakdown of silver/silver-nickel alloy in a 1.4^{-4} Pa vacuum is approximately 2-4$\times 10^9$ V/m with a negligible leakage current [70]. Other high-voltage designs for low-mass scalar-type dark matter [71] and axion-monopole search [72] have been proposed recently.

Benchmark C shows that an electric field strength in the order of GVm^{-1} would be required to touch down to the theoretical prediction for the (KSVZ) QCD axion. While a GVm^{-1} E-field could still be sustained by strong and transparent insulation material (such as diamond), achieving such a colossal voltage over a large distance is a challenge to high-voltage engineering, and here it is only shown for illustrative purposes. As shown in Eq. (8), the sensitivity improves toward larger m_a, but it has its coherence limit: the diameter of the electrified cylinder should not exceed the half-wavelength of the induced electromagnetic wave $\lambda_\gamma = m_a^{-1}/2$, or $8R_1 > \lambda_a$.

As shown in Eq. (8), increasing the cylinder size and/or the electric field strength is efficient for improving the $g_{a\gamma}$

sensitivity. This corresponds to a stronger induced $\vec{B}_a$ field. Improvements from more pickup coil turns, lowering the noise temperature and a longer observation time are less effective. The $g_{a\gamma}$ limit scales with the quality factor as $Q^{-3/4}$, which shows the necessity of exploiting the dark matter's coherence via proper frequency filtering.

4 Summary and discussion

In this paper we explore the concept of a narrow-band axionic dark matter detection scheme with a strong laboratory static electric field as the $a \rightarrow \gamma$ converting medium. The geometry of a cylindrical capacitor allows the axion-induced effective current to form a solenoid pattern and yield a concentrated magnetic field signal in the inner region of the capacitor. As axion-photon conversion is suppressed by axion velocity under a static electric field, we adopt a narrow band approach to enhance signal detection. Working at relatively long wavelengths, an LC resonance offers front-end high Q-factor frequency filtering, which can be matched to the dark matter field's energy dispersion. The high Q-factor allows the signal to build up in the LCR circuit that effectively enhances the signal strength, and can be probed by cryogenic amplifiers and detectors with high sensitivity.

We propose three benchmark scenarios, and demonstrate that a submeter capacitor scheme with mainstream cryogenic technology is sensitive to $g_{a\gamma} \sim 10^{-12}$ GeV^{-1}. For a multimeter cylindrical capacitor and mK-level noise temperature, the projected sensitivity can be further improved to the 10^{-15} GeV^{-1} scale with 10 MVm^{-1} static E field strength. The theoretical QCD axion prediction requires a high field $E \sim \mathcal{O}(10^9)$ Vm^{-1} setup that involves further R&D on implementing high dielectric materials.

In addition to avoiding magnetic fluctuations, the absence of a strong magnetic field allows the pickup coils to use superconductor materials as an option to reduce the LCR circuit's resistance, and in principle low-resistance material needs to be used when $\omega L/Q$ is small. For thermal noise control, only the circuit parts with resistance need to be restricted to the lowest ($\sim$mK) temperature. Given the meter-scale size of the cylinder, this reduces the overall cooling requirement of the system.

Due to the direction dependence in the effective $\vec{j}_a = -g_{a\gamma} a \vec{E} \times \vec{k}_a$, the signal strength with a static electric field is modulated by both the axion field periodicity and apparatus orientation. Adjustment of capacitor direction, as well as daily modulation, can be used as an additional method of differentiation of the axion-induced signal from the system's own systematics.

Data Availability Statement This manuscript has no associated data or the data will not be deposited. [Authors' comment: This research consists of theoretical discussions of a conceptual haloscope experiment desgin and it has no associated measurement data].

References

1. P.A.R. Ade et al., Planck 2015 results. XIII. Cosmological parameters. Astron. Astrophys. **594**, A13 (2016)
2. M.S. Turner, Coherent scalar field oscillations in an expanding universe. Phys. Rev. D **28**, 1243 (1983)
3. R.D. Peccei, H.R. Quinn, CP, conservation in the presence of instantons. Phys. Rev. Lett. **38**, 1440–1443 (1977) (**328(1977)**)
4. S. Weinberg, A new light boson? Phys. Rev. Lett. **40**, 223–226 (1978)
5. F. Wilczek, Problem of strong P and T invariance in the presence of instantons. Phys. Rev. Lett. **40**, 279–282 (1978)
6. R.D. Peccei, H.R. Quinn, Constraints imposed by CP conservation in the presence of instantons. Phys. Rev. D **16**, 1791–1797 (1977)
7. J.E. Kim, Weak interaction singlet and strong CP invariance. Phys. Rev. Lett. **43**, 103 (1979)
8. M.A. Shifman, A.I. Vainshtein, V.I. Zakharov, Can confinement ensure natural CP invariance of strong interactions? Nucl. Phys. B **166**, 493–506 (1980)
9. A.R. Zhitnitsky, On possible suppression of the axion hadron interactions. (In Russian). Sov. J. Nucl. Phys. **31**, 260 (1980) (**Yad. Fiz.31,497(1980)**)
10. M. Dine, W. Fischler, M. Srednicki, A simple solution to the strong CP problem with a harmless axion. Phys. Lett. **104B**, 199–202 (1981)
11. R.D. Peccei, The strong CP problem and axions. Lect. Notes Phys. **741**, 3–17 (2008)
12. J.E. Kim, G. Carosi, Axions and the strong CP problem. Rev. Mod. Phys. **82**, 557–602 (2010). (**Erratum: Rev. Mod. Phys. 91, 049902 (2019)**)
13. R.J. Crewther, P. Di Vecchia, G. Veneziano, E. Witten, Chiral estimate of the electric dipole moment of the neutron in quantum chromodynamics. Phys. Lett. B **88**, 123 (1979) (**Erratum: Phys. Lett. B 91, 487 (1980)**)
14. C.G. Callan Jr., R.F. Dashen, D.J. Gross, Toward a theory of the strong interactions. Phys. Rev. D **17**, 2717 (1978)
15. C. Vafa, E. Witten, Parity conservation in QCD. Phys. Rev. Lett. **53**, 535 (1984)
16. J. Preskill, M.B. Wise, F. Wilczek, Cosmology of the invisible axion. Phys. Lett. B 120:127–132 (1983) (**URL(1982)**)
17. L.F. Abbott, P. Sikivie, A cosmological bound on the invisible axion. Phys. Lett. B **120**, 133–136 (1983) (**URL(1982)**)
18. M. Dine, W. Fischler, The not so harmless axion. Phys. Lett. B **120**, 137–141 (1983)
19. P. Sikivie, Of axions, domain walls and the early universe. Phys. Rev. Lett. **48**, 1156–1159 (1982)
20. J. Ipser, P. Sikivie, Are galactic halos made of axions? Phys. Rev. Lett. **50**, 925 (1983)
21. P. Sikivie, Axion cosmology. Lect. Notes Phys. **741**, 19–50 (2008)
22. M.P. Hertzberg, M. Tegmark, F. Wilczek, Axion cosmology and the energy scale of inflation. Phys. Rev. D **78**, 083507 (2008)
23. C. Bartram et al., Search for invisible axion dark matter in the 3.3–4.2 μeV mass range. Phys. Rev. Lett. **127**(26), 261803 (2021)
24. L. Zhong et al., Results from phase 1 of the HAYSTAC microwave cavity axion experiment. Phys. Rev. D **97**(9), 092001 (2018)
25. O. Kwon et al., First results from an axion haloscope at CAPP around 10.7 μeV. Phys. Rev. Lett. **126**(19), 191802 (2021)
26. B.T. McAllister, G.R. Flower, M. Goryachev, J. Bourhill, E.N. Ivanov, M.E. Tobar, The ORGAN experiment: first results and future plans, in *13th Patras Workshop on Axions, WIMPs and WISPs* (2018), p. 75–78
27. A. Álvarez Melcón et al., First results of the CAST-RADES haloscope search for axions at 34.67 μeV. JHEP **21**, 075 (2020)
28. D. Alesini et al., Search for invisible axion dark matter of mass $m_a = 43$ μeV with the QUAX-$a\gamma$ experiment. Phys. Rev. D **103**(10), 102004 (2021)
29. H. Chang et al., First results from the Taiwan axion search experiment with a haloscope at 19.6 μeV. Phys. Rev. Lett. **129**(11), 111802 (2022)
30. Y. Oshima, H. Fujimoto, M. Ando, T. Fujita, Y. Michimura, K. Nagano, I. Obata, T. Watanabe, Dark matter axion search with riNg cavity experiment DANCE: current sensitivity, in *55th Rencontres de Moriond on Gravitation*, 5 (2021)
31. C.P. Salemi, First results from ABRACADABRA-10cm: a search for low-mass axion dark matter, in *54th Rencontres de Moriond on Electroweak Interactions and Unified Theories*, pages 229–234, (2019)
32. X. Li, MADMAX: a dielectric haloscope experiment. *PoS*, ICHEP2020, 645 (2021)
33. J. Liu et al., Broadband solenoidal haloscope for terahertz axion detection. Phys. Rev. Lett. **128**(13), 131801 (2022)
34. I.G. Irastorza, J. Redondo, New experimental approaches in the search for axion-like particles. Prog. Part. Nucl. Phys. **102**, 89–159 (2018)
35. P. Sikivie, Invisible axion search methods. Rev. Mod. Phys. **93**(1), 015004 (2021)
36. P. Sikivie, Experimental tests of the invisible axion. Phys. Rev. Lett. 51:1415–1417 (1983) (**Erratum: Phys.Rev.Lett. 52, 695 (1984)**)
37. Q. Yang, Y. Gao, Z. Peng, Quantum dual-path interferometry scheme for axion dark matter searches **1** (2022)
38. P. Svrcek, E. Witten, Axions in string theory. JHEP **06**, 051 (2006)
39. R. Barbieri, R.N. Mohapatra, D.V. Nanopoulos, D. Wyler, Aspects of a superlight grand unified axion. Phys. Lett. B **107**, 80–84 (1981)
40. G.F. Giudice, R. Rattazzi, A. Strumia, Unificaxion. Phys. Lett. B **715**, 142–148 (2012)
41. L.J. Hall, Y. Nomura, S. Shirai, Grand unification, axion, and inflation in intermediate scale supersymmetry. JHEP **06**, 137 (2014)
42. A. Ernst, A. Ringwald, C. Tamarit, Axion predictions in $SO(10) \times U(1)_{PQ}$ models. JHEP **02**, 103 (2018)
43. Y. Gao, T. Li, Q. Yang, The minimal UV-induced effective QCD axion theory. 12 (2019)
44. A.V. Gramolin, D. Aybas, D. Johnson, J. Adam, A.O. Sushkov, Search for axion-like dark matter with ferromagnets. Nat. Phys. **17**(1), 79–84 (2021)

45. N. Crisosto, P. Sikivie, N.S. Sullivan, D.B. Tanner, J. Yang, G. Rybka, Admx slic: results from a superconducting lc circuit investigating cold axions. Phys. Rev. Lett. **124**, 241101 (2020)

46. J.A. Devlin, M.J. Borchert, S. Erlewein, M. Fleck, J.A. Harrington, B. Latacz, J. Warncke, E. Wursten, M.A. Bohman, A.H. Mooser, C. Smorra, M. Wiesinger, C. Will, K. Blaum, Y. Matsuda, C. Ospelkaus, W. Quint, J. Walz, Y. Yamazaki, S. Ulmer, Constraints on the coupling between axionlike dark matter and photons using an antiproton superconducting tuned detection circuit in a cryogenic penning trap. Phys. Rev. Lett. **126**, 041301 (2021)

47. L. Brouwer et al., Proposal for a definitive search for GUT-scale QCD axions. Phys. Rev. D **106**(11), 112003 (2022)

48. B. Cabrera, S. Thomas, Talk at 'Axions 2010' workshop, Gainesville, Florida, USA, Jan 15-17, 2010. see: http://www.phys.ufl.edu/research/Axions2010/presentations.html and http://www.physics.rutgers.edu/~scthomas/talks/Axion-LC-Florida.pdf

49. P. Sikivie, N. Sullivan, D.B. Tanner, Proposal for axion dark matter detection using an LC circuit. Phys. Rev. Lett. **112**(13), 131301 (2014)

50. Y. Gao, Q. Yang, Broadband dark matter axion detection using a cylindrical capacitor. 12 (2020)

51. P. Sikivie, Q. Yang, Bose–Einstein condensation of dark matter axions. Phys. Rev. Lett. **103**, 111301 (2009)

52. L. Hui, J.P. Ostriker, S. Tremaine, E. Witten, Ultralight scalars as cosmological dark matter. Phys. Rev. D **95**(4), 043541 (2017)

53. J. Ouellet, Z. Bogorad, Solutions to axion electrodynamics in various geometries. Phys. Rev. D **99**(5), 055010 (2019)

54. Yu. Junxi Duan, C.-Y.J. Gao, S. Sun, Y. Yao, Y.-L. Zhang, Resonant electric probe to axionic dark matter. Phys. Rev. D **107**(1), 015019 (2023)

55. A. Berlin, R.T. D'Agnolo, S.A.R. Ellis, C. Nantista, J. Neilson, P. Schuster, S. Tantawi, N. Toro, K. Zhou, Axion dark matter detection by superconducting resonant frequency conversion. JHEP **07**(07), 088 (2020)

56. M. Simanovskaia, Design, fabrication, and characterization of a high-frequency microwave cavity for HAYSTAC. Ph.D. thesis, UC, Berkeley (main) (2020)

57. L. Steffen, D. Bozyigit, C. Lang et al., Antibunching of microwave-frequency photons observed in correlation measurements using linear detectors. Nat. Phys. **7**, 154–158 (2011)

58. Z.H. Peng, S.E. de Graaf, J.S. Tsai, O.V. Astafiev, Tuneable on-demand single-photon source in the microwave range. Nat. Commun. **7**(1) (2016)

59. B.T. Mcallister, S.R. Parker, E.N. Ivanov, M.E. Tobar, Cross-correlation signal processing for axion and WISP dark matter searches. IEEE Trans. Ultrason. Ferroelectr. Freq. Control **66**(1), 236–243 (2019)

60. C. Hagmann, P. Sikivie, N. Sullivan, D.B. Tanner, S.I. Cho, Cavity design for a cosmic axion detector. Rev. Sci. Instrum. **61**, 1076–1085 (1990)

61. J.W. Foster, N.L. Rodd, B.R. Safdi, Revealing the dark matter halo with axion direct detection. Phys. Rev. D **97**(12), 123006 (2018)

62. M. Lisanti, M. Moschella, W. Terrano, Stochastic properties of ultralight scalar field gradients. Phys. Rev. D **104**(5), 055037 (2021)

63. D. Budker, P.W. Graham, M. Ledbetter, S. Rajendran, A. Sushkov, Proposal for a cosmic axion spin precession experiment (CASPEr). Phys. Rev. X **4**(2), 021030 (2014)

64. V. Anastassopoulos et al., New CAST limit on the axion-photon interaction. Nat. Phys. **13**, 584–590 (2017)

65. P. Sha, W.-M. Pan, S. Jin, J.-Y. Zhai, Z.-H. Mi, B.-Q. Liu, C. Dong, F.-S. He, R. Ge, L.-R. Sun, S.-A. Zheng, L.-X. Ye, Ultrahigh accelerating gradient and quality factor of cepc 650 mhz superconducting radio-frequency cavity. Nucl. Sci. Tech. **33**, 095005 (2022)

66. F. He, W. Pan, P. Sha, J. Zhai, Z. Mi, X. Dai, S. Jin, Z. Zhang, C. Dong, B. Liu, H. Zhao, R. Ge, J. Zhao, Z. Mu, L. Du, L. Sun, L. Zhang, C. Yang, X. Zheng, Medium-temperature furnace baking of 1.3 ghz 9-cell superconducting cavities at ihep. Supercond. Sci. Technol. **34**(9), 095005 (2021)

67. A.E. Vlieks, M.A. Allen, R.S. Callin, W.R. Fowkes, E.W. Hoyt, J.V. Lebacqz, T.G. Lee, Breakdown phenomena in high-power klystrons. IEEE Trans. Electr. Insul. **24**(6), 1023–1028 (1989)

68. H.C. Miller, Flashover of insulators in vacuum: review of the phenomena and techniques to improved holdoff voltage. IEEE Trans. Electr. Insul. **28**, 512–527 (1993)

69. P.D. Lin, H.C. Ye, G.D. Wilk, Leakage current and breakdown electric-field studies on ultrathin atomic-layer-deposited Al_2O_3 on GaAs. Appl. Phys. Lett. **87**, 182904 (2005)

70. N. Zouache, A. Lefort, Electrical breakdown of small gaps in vacuum. IEEE Trans. Dielectr. Electr. Insul. **4**, 358 (1997)

71. V.V. Flambaum, B.T. McAllister, I.B. Samsonov, M.E. Tobar, Searching for scalar field dark matter using cavity resonators and capacitors. Phys. Rev. D **106**(5), 055037 (2022)

72. M.E. Tobar, A.V. Sokolov, A. Ringwald, M. Goryachev, Searching for GUT-scale QCD axions and monopoles with a high-voltage capacitor. Phys. Rev. D **108**(3), 035024 (2023)